In-phase synchronization between two auto-oscillating bubbles

Dang Minh Nguyen,[1,2] Muttikulangara Swaminathan Sanathanan,[3] Jianmin Miao,[3] David Fernandez Rivas,[4] and Claus-Dieter Ohl[1,2]

[1]*Division of Physics and Applied Physics, School of Physical and Mathematical Sciences, Nanyang Technological University, Singapore 637371*

[2]*Institute for Physics, Otto-von-Guericke University, Magdeburg 39106, Germany*

[3]*School of Mechanical and Aerospace Engineering, Nanyang Technological University, Singapore 639798*

[4]*Mesoscale Chemical Systems, Faculty of Science and Technology, University of Twente, 7500 AE Enschede, The Netherlands*

(Received 5 November 2018; published 22 April 2019)

Acoustically driven bubbles are nonlinear oscillators showing a wide range of behaviors such as period-doubling bifurcations, deterministic chaos, and synchronization to an external signal. Here we demonstrate that bubbles driven with a constant heat source can couple with each other and yield in-phase synchronization, even in the absence of an external sound field. Besides perfect synchronization, we resolve the parameter space where independent oscillations and bubble merging occur. The main finding that only weakly driven oscillating bubbles synchronize provides a path for experimental scale-up to study spatiotemporal synchronization. In the wider scope the findings are relevant for heat transfer applications from structured heaters where complex multibubble oscillations are expected.

DOI: 10.1103/PhysRevFluids.4.043601

I. INTRODUCTION

Bubbles in liquids are nonlinear oscillators and when driven by an external sound field they reveal period-doubling bifurcation and acoustic chaos [1]. A fascinating example of the mutual interaction between bubbles besides deterministic chaos is the formation of filamentary structures resembling Lichtenberg figures of electrical discharges [2–4]. At the heart of these spatiotemporal structures is the mutual interaction between neighboring bubbles. While the interaction of many bubbles has received a great deal of interest [5–19], the study of the specific interaction between two oscillating bubbles remains an experimental challenge [5,9,13,16–18]. Besides experimental complexity, a more fundamental problem is that the acoustic interaction of two bubbles is clouded by the external sound field driving the bubbles into oscillations. So far all studies on this interaction and synchronization between nonlinear bubble oscillators have been obscured by the presence of the external forcing, which prescribes a phase and frequency for both oscillators [20]. Here we report an experimental realization of two coupled bubble oscillators where this problem is avoided: The energy is provided from constant heat sources driving each bubble into auto-oscillations. As a result, we have an experimental system with two nonlinear oscillators that only through their mutual interaction obtain an in-phase synchronization [21] at their self-selected frequency.

Once a bubble is nucleated on the surface of the submerged microheater, it exhibits volume oscillations. We have recently demonstrated an electric version of the microheater [22], which improves the control over size and input energy as compared to an earlier laser-based heater [23]. The cyclic vaporization of liquid for a brief time interval (approximately 30 ns) at minimum bubble volume supplies the necessary heat input to overcome the energy dissipation of the system caused mainly by viscosity and acoustic radiation. Surprisingly, once the oscillations have set in, they continue stably for millions of cycles.

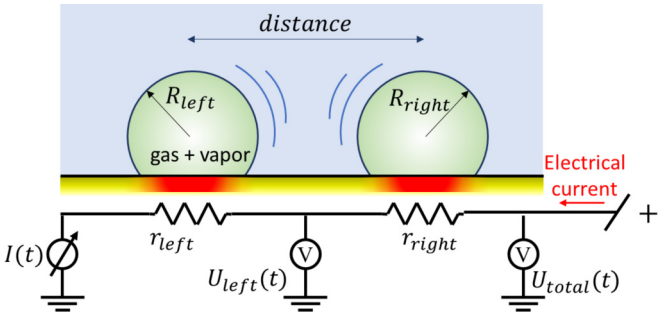

FIG. 1. Sketch of the experiment to generate and monitor two auto-oscillating bubbles on two closely placed electrical microheaters.

In the present work we bring two oscillate-boiling bubbles into close proximity and study their mutual interaction. It should be noted that the frequency and phase of oscillations are not prescribed by an external source, but the auto-oscillator, i.e., each bubble, is free to choose. The experimental control parameters are the distance and the electrical power supplied to the heaters. The coupled oscillations are characterized with high-speed photography, recording of the acoustic emissions, and instantaneous temperature measurements.

II. MATERIALS AND METHODS

The electrical heater design for two bubbles follows Ref. [22], i.e., with a 50-nm thin film of platinum deposited on a glass substrate and connected to a 600-nm-thick gold layer supplying the electrical current. The electrical connections and locations of the generated bubbles are sketched in Fig. 1. The two heaters have an area of $10 \times 10\ \mu\text{m}^2$ each and are connected in series. The electrical power is provided by a constant electrical current supply (Thorlabs LDC 220). While the power delivered to each heater should theoretically be the same, we observe small deviations as their individual resistance are not strictly equal. During the experiment the voltages across each heater and the current I are monitored with a 12-bit oscilloscope (Lecroy HRO 64Zi). The memory of the oscilloscope allows us to monitor the instantaneous temperature and power of each heater for several 100 000 oscillations.

The glass chip with the heaters is attached to the bottom of an acrylic container ($10 \times 10 \times 10\ \text{mm}^3$) forming the test section. Two faces of the container are replaced with microscopic glass slides for better imaging with the high-speed camera (Photron SA-X2) running at 300 000 frames per second. A long distant objective lens (20× PTEM M Plan Apo, Edmund Optics) provides a final resolution of 1 μm per camera pixel. Besides the electrical signals, also the acoustic emission from the bubble oscillation is recorded with a hydrophone (ONDA HNR1000). The timing of the experimental devices is synchronized with a digital pulse generator (BNC 575, Berkeley Nucleonics). The detailed setup is presented in Fig. 2.

Previously, it was found that an individual oscillate-boiling bubble either may oscillate stably for many million cycles or stops oscillating within tens of milliseconds [22]. The stable oscillate-boiling mode is only found above a certain power threshold, which in turn depends on the size of the heater, i.e., 20 mW for a $10 \times 10\ \mu\text{m}^2$ heater. In each cycle the bubble pinches off a microbubble from its apex and rapidly cools the heater with a liquid jet impact during the bubble collapse. The other mode termed unstable oscillate boiling lacks the pinch-off and therefore, due to rectified diffusion, the bubble grows steadily. With time, the frequency of oscillation decreases and eventually the oscillation ceases. Due to the missing jet impact, the temperature of the heater remains approximately constant over a cycle. All experiments are conducted at an electrical power

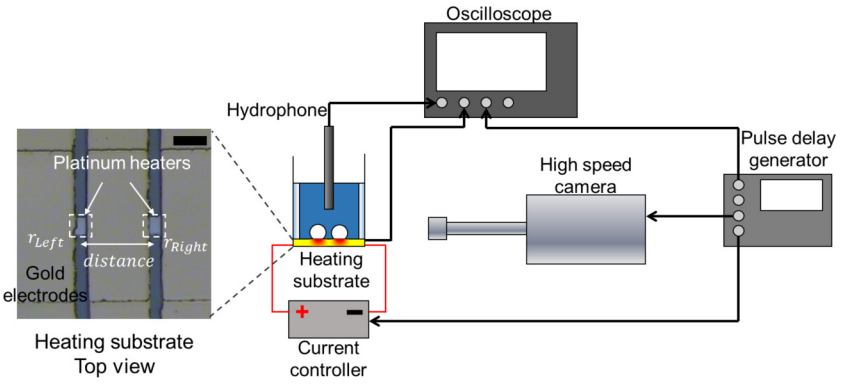

FIG. 2. Full experimental setup that studies the system of two oscillate-boiling bubbles. The black arrows represent signal transmission and the red lines represent power supply connections. The scale bar in the heater's top view represents 20 μm.

of more than 20 mW. For an individual bubble this would always result in the stable oscillating mode.

To limit thermal stress and damage to the heaters, we run the experiment for a short time of up to only 0.5 s.

III. EXPERIMENTAL RESULTS

A. In-phase synchronization

We report first the bubble dynamics at an intermediate distance of 40 μm and at a relative high electrical power of approximately 35 mW for each heater. The findings are summarized in Fig. 3. In Fig. 3(a), selected frames in the upper row depict the oscillations of the two bubbles recorded shortly after the start of the experiment and in the row below a few milliseconds later. Due to small differences in the heaters, the two bubbles have a slightly different size and nucleation time, resulting in different oscillation periods and phases of oscillations. Over time, however, the two bubbles synchronize their oscillations and they both reach in each cycle a maximum radius of approximately 10 μm. The temporal development leading to this synchronization is revealed in the spectrogram of their acoustic emission below. There in Fig. 3(b) around $t = 1.5$ ms, two distinct frequencies and their higher harmonics are noticeable. The initially (on average) smaller left bubble oscillates at a higher frequency (above 200 kHz), while the larger right bubble oscillates at the lower frequency (below 200 kHz). From $t = 3.5$ ms, as indicated with the vertical dashed line, both bubbles synchronize into a single frequency. Thereafter the frequency remains about constant before it steadily decreases over time. The equivalent radius (to that of a hemisphere) of each bubble is plotted in Fig. 3(c) in green and blue. Initially, at time $t = 1$ ms, their radii differ in phase, but from $t = 3.5$ ms the smaller bubble (blue line) follows the phase of the larger bubble and their time series become nearly indistinguishable [see the inset in Fig. 3(c)]. In other experiments, we observe some differences between the bubbles' radii, yet their phases are still perfectly synchronized. Both bubbles then increase slowly in size, which is consistent with the decrease in frequency seen in Fig. 3(b). Due to this growth, the liquid contact lines expand. Yet instead of a symmetrical expansion they move closer towards each other and thereby decrease the distance between their centers of mass [red line in Fig. 3(c)]. This movement can be explained by the attractive secondary Bjerknes force for in-phase oscillating bubbles [8] and by the spreading of the heating region (see Sec. IV). The in-phase synchronization of the two bubbles is a remarkable dynamic feature, which is nicely confirmed by plotting the correlation coefficient of their instantaneous radius [see Fig. 3(d)]. Note that, in the synchronization case, both bubbles oscillate in the unstable mode, which is indicated by

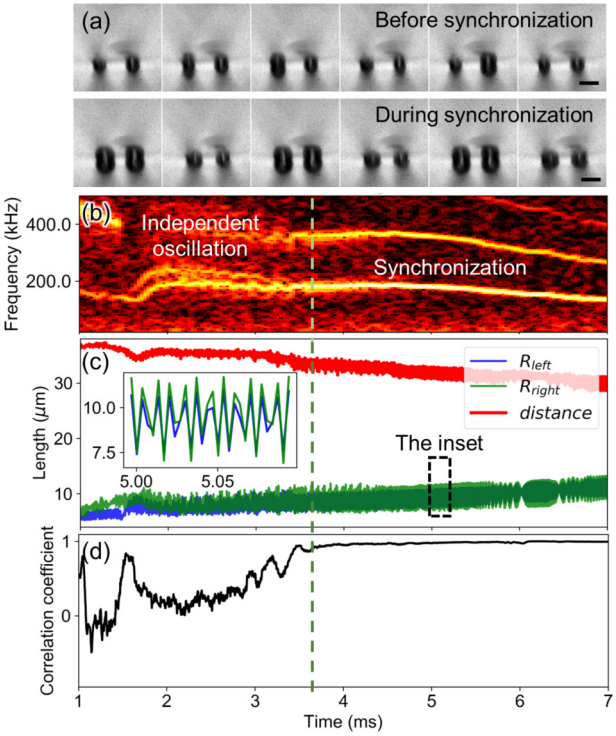

FIG. 3. Two synchronized oscillate-boiling bubbles. Here the distance between heaters is 40 μm. The power of the left and the right heater is 34.9 and 36.0 mW, respectively. (a) Captured images before and during the time when two bubbles synchronize. A digital filter was applied to remove dirt in the background. Refer to video 2 in [24] for the raw data. The time between two consecutive frames is 3.33 μs. The scale bar shows 20 μm. (b) Spectrogram of the acoustic signal emitted from two synchronized oscillate-boiling bubbles. (c) Distance between the bubbles' centers of mass and their effective radii retrieved from the recording. (d) Correlation coefficient between the effective radii of the two bubbles, calculated with a window time of 100 μs, i.e., 30 frames of the recordings.

the absence of the microbubble pinch-off and the periodic temperature oscillation of the heater (see Appendix A).

By changing the distance and electric power, the qualitatively different behavior of the two-bubble system can be observed. We start with bubbles separated farther apart at a distance of 50 μm (see Fig. 4). Unlike the synchronization case, here both bubbles operate in the stable oscillating mode, i.e., with microbubble pinch-off. With the start of the electrical current, the two vapor bubbles start oscillating and each reaches a stable maximum radius at a constant frequency. During each cycle they release a microbubble from their apexes and induce a rapid cooling on their corresponding heater. The acoustic and temperature spectrograms show very similar features (see Appendix A). In particular, the acoustic spectrogram reveals a superposition of two distinct frequencies [Fig. 4(b)], an indication that the two bubbles do not synchronize and therefore the time series of their bubble radii in Fig. 4(c) are uncorrelated.

By increasing the heating power, the system reveals a third regime: The bubbles oscillate only for a few cycles while their average radius grows with time before they eventually merge. Here the oscillation is unstable with no microbubble pinch-off, no periodic cooling of the heater, and no synchronization. This radically different regime is reflected in the images and the spectrogram of the acoustic signal shown in Fig. 5 [24].

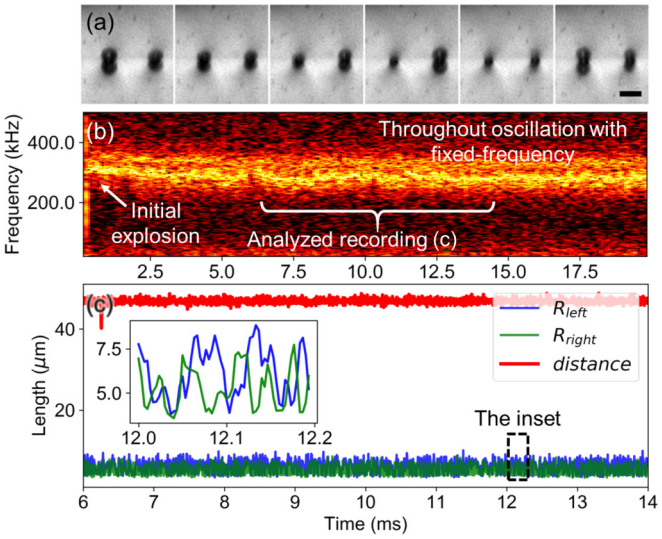

FIG. 4. Two stable oscillate-boiling bubbles (see video 1 in [24]). Here the distance between two heaters is 50 μm. The power of the left and the right heater is 25.4 and 25.1 mW, respectively. (a) Captured images of the bubble dynamics. The sizes of the pinch-off bubbles are close to the optical resolution, so they are barely noticeable. The time between two consecutive frames is 3.33 μs. The scale bar represents 20 μm. (b) Spectrogram of the acoustic signal emitted from the two bubbles. (c) Distance of the bubbles' centers of mass and their effective radii retrieved from the recording during the period marked in (b). The inset shows a close-up of the data in the black rectangle.

B. Parameter space

As previously mentioned, we find that the dynamics of two neighboring oscillating bubbles falls in one of three distinct regimes. Bubbles sufficiently close together and driven at an intermediate power synchronize perfectly, bubbles farther apart oscillate independently, and further increasing the power at short distance results in the merging of the bubbles. Figure 6 reveals the regions in the parameter plot where in-phase synchronization is achieved, i.e., distances between 40 and 50 μm and powers between 32 and 42 mW. At larger distance most bubbles fall into the independent oscillating regime, while they merge at closer distance and at high driving [24].

IV. DISCUSSION

A. Why only unstable oscillate-boiling bubbles synchronize

The two bubbles couple through the flow field and the acoustic emissions. To understand the physics of the process we use a simple model based on potential flow which ignores the boundary layers and finite sound speed of the two-bubble system [8,26]. The solution of the problem leads to a pressure interaction term p_i between two neighboring (hemi)spherical bubbles in the Rayleigh-Plesset equation

$$p_i = \rho d^{-1}(R^2\ddot{R} + 2R\dot{R}^2), \tag{1}$$

where R is the bubble radius, d the distance, and ρ the density of the liquid. In stable oscillate boiling the liquid jet impact prematurely disrupt the bubble's natural collapse, causing rapid vaporization and rapid reexpansion of the bubble driven by the expanding vapor [22,23]. The pressure interaction from the neighboring bubble is therefore not sufficient to overcome this violent mechanism. In contrast, the unstable mode is driven by a more gentle bubble's inertia and can be affected by the acoustic emission.

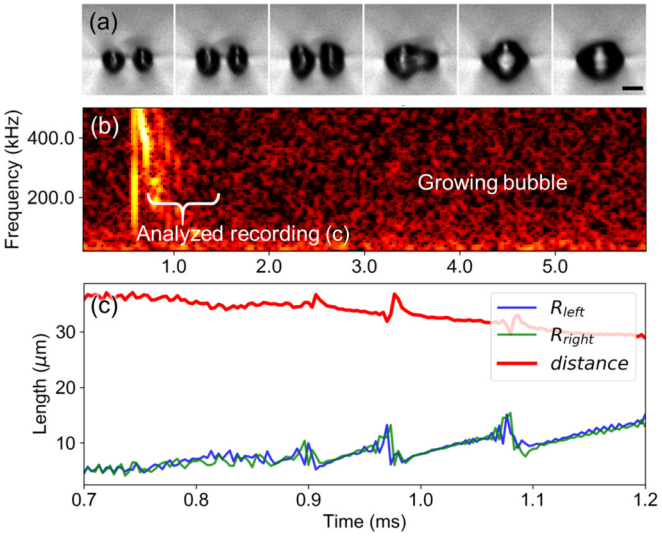

FIG. 5. Two bubbles grow and merge. Here the distance between two heaters is 40 μm. The power of the left and the right heater is 48.0 and 47.7 mW, respectively. (a) Captured images when two bubbles grow and merge (see video 3 in [24]). The time between two consecutive frames is 33.3 μs. The scale bar shows 20 μm. (b) Spectrogram of the acoustic signal emitted from two growing bubbles. (c) Distance of the bubbles' centers of mass and their effective radii retrieved from the recording.

To support this hypothesis, we extend our model [23] with the interaction term p_i. For the unknowns R_i and temperature T_i with $i = 1, 2$ numbering the bubble, we solve the coupled Keller-Miksis equation [27] and the energy equation for the gas or vapor inside the bubbles. To mimic the thermal kick received during the jet impact in stable oscillate boiling, the input power is approximated with a step function. More specifically, the bubble receives the full power from the heater if its radius is smaller than a certain threshold (during the jet impact) and otherwise this term is zero. The value of this threshold can be derived from the power law (6.1) in Ref. [28]. For the unstable

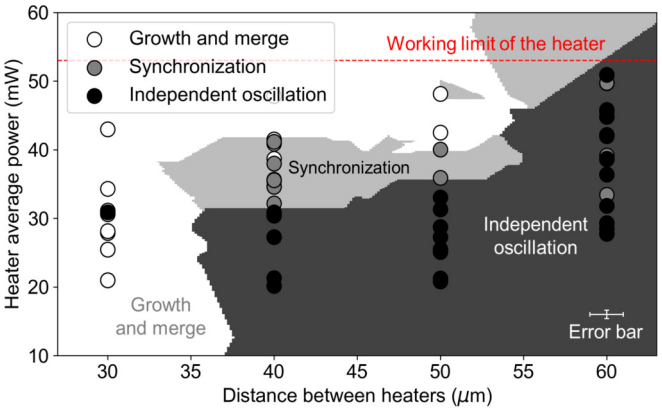

FIG. 6. Parameter space of two nearby oscillate-boiling bubbles as a function of different heating powers and distances between heaters. All data points share the same error bar, which is plotted separately. The classification region is constructed using the k-nearest-neighbor algorithm [25] with $k = 5$.

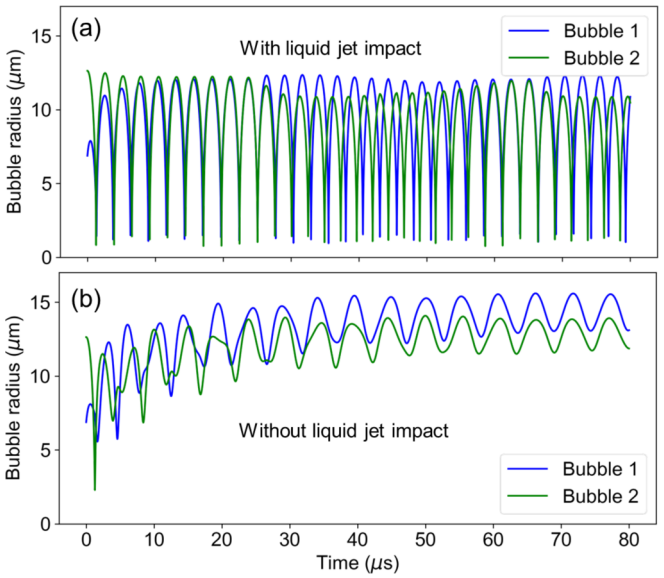

FIG. 7. Numerical calculation of two closely placed bubbles, both operating in (a) stable oscillate-boiling mode with liquid jet impact and (b) unstable oscillate-boiling mode without liquid jet impact. Here the power supplied to bubble 1 is 34 mW and to bubble 2 is 30 mW and their distance is 40 μm.

mode without the jet, a slower energy transport is represented with a smoothed function where the input power is inversely proportional to the instantaneous bubble's radius (see Appendix B).

In the absence of the interaction term p_i we find two qualitatively different modes of oscillation. For the steplike driving, the bubble undergoes large volume oscillations with rapid collapses. In contrast, the smoothed profile after some transient time results in an approximately harmonic bubble oscillation around an equilibrium radius (see Appendix B for the numerical result of a single bubble).

Figure 7 presents the radius versus time curves for the strongly collapsing (stable) and mildly oscillating (unstable) bubbles when the interaction term is switched on. In the strong oscillation regime [see Fig. 7(a)], the two bubbles oscillate at different frequencies and therefore their phases drift with time. When both bubbles oscillate at a smaller amplitude [Fig. 7(b)] they oscillate synchronously with the same frequency after a brief transient. The model provides qualitatively similar features of independent and synchronous oscillations as in the experiments described above. The model also predicts that the bubble oscillation frequency in the coupled mode is lower than in the independent mode. Yet for a more complete understanding, the mass transport into the bubble through rectified diffusion should be accounted for [24].

B. Connections between bubble distance, heating power, and synchronization mode

Placing two heaters in close proximity results in the spreading of some of the heat between the heaters in the substrate. Thereby the effective microheater size is enlarged as compared to the isolated microheater. In Ref. [22] we reported that the regime of stable oscillate-boiling requires a higher power when the heater size is increased, i.e., from 10×10 to 15×15 μm^2. Thus, while at a certain power an individual heater operates in the stable oscillate-boiling regime, it shifts to the unstable regime when accompanied by a second microheater, which then leads to synchronization. At even higher electrical power we also observed the merging of two bubbles. Besides the secondary Bjerknes force, a more subtle explanation may be that this thermal spreading forms a heat bridge between the heaters and merges them into one big heating spot.

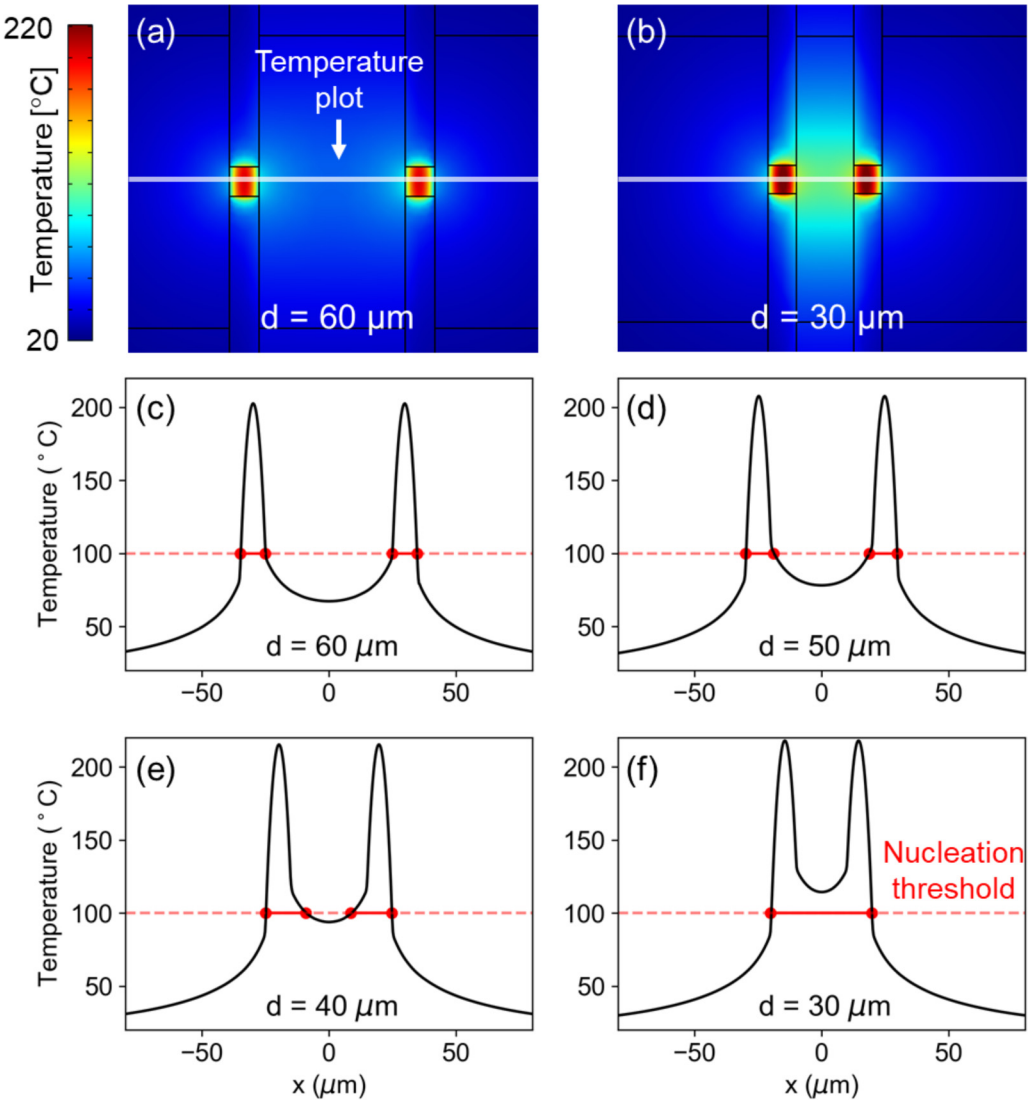

FIG. 8. Temperature distribution of the substrate at 1 ms after the current is triggered. Here each heater is operated at 35 mW and placed at four different distances following the experiment. (a) and (b) Top view of the thermal profile of the substrate with the longest and shortest distances. (c)–(f) Temperature distribution along the white line with different distances of the heaters.

Figure 8 shows the simulated thermal profile of the heater at 1 ms after the current is triggered. This is the typical timescale for the bubbles to settle in either unstable or stable oscillation. Here we approximate the boiling point of water, i.e., 100 °C, to be a threshold above which the heater becomes a nucleation spot that favors the formation of bubbles. It can be seen that as the heaters are closer to each other, the thermal spreading effect becomes more significant and enlarges the effective nucleation size. The unstable regime is therefore more likely to occur. When the distance is reduced to $d = 30$ μm, the heating regions connect, giving the bubbles a tendency to merge. This thermal spreading effect may explain why the parameter region of synchronization is limited to intermediate distances and intermediate heating powers.

C. Benefits of nonsynchronicity for thermal application

Oscillate boiling shows improved heat transfer efficiency compared to nucleate boiling [22,23]. Towards application, this phenomenon needs to be scaled up or numbered up to multiple oscillate-boiling bubbles covering the whole heating floor. Our results show that if placed sufficiently close, those bubbles might synchronize, but then shortly after they will grow, merge, and become just nucleate boiling bubbles. This severely limits the intended outcome. To maintain a system of longer operation time, oscillate boiling should be in the stable mode (with microbubble streaming, periodic cooling, and no synchronization). The results presented in Fig. 6 provide the design criteria for the scaled-up heating device, i.e., the suitable distance between individual heating elements, maximum operating power, etc.

V. CONCLUSION

In summary, the self-driven nature of oscillate boiling has allowed us to resolve the mutual interactions of two oscillating bubbles in the absence of an external field. Thus, without imposing a frequency or phase, the bubbles obtain in-phase synchronization. In addition, we have identified two more interaction regimes: independent oscillations at far distances and merging for small distances and strong heating. Our main finding is that only mildly oscillating bubbles synchronize, while large-amplitude oscillations result in independent oscillations. The former are driven by a lower peak power, while the latter are the result of higher-power impulsive kicks. If we extrapolate our results to acoustically driven bubbles, it would suggest that bubbles at moderate driving may synchronize mutually, while at higher amplitude they follow the external sound field at their specific phase. Whether that holds for continuous driving remains to be shown. The results also provide design criteria for scaling up this phenomenon for thermal application, in which the heating floor will be covered by many independent, nonsynchronized oscillate-boiling bubbles.

ACKNOWLEDGMENTS

We thank Hu Liangxing and Stefan Schlautmann for their help with the fabrication of the samples and Ulrich Parlitz for his insights into synchronization. This research was supported by Ministry of Education Singapore (Tier 1 Grant No. RG90/15). D.F.R. acknowledges the support by The Netherlands Centre for Multiscale Catalytic Energy Conversion (MCEC), an NWO Gravitation programme funded by the Ministry of Education, Culture and Science of the government of The Netherlands.

APPENDIX A: SPECTROGRAM OF ACOUSTIC PRESSURE AND THE HEATER'S TEMPERATURE

Figure 9 shows a typical spectrogram of the emitted acoustic signal and the temperature of each heater in the regime where two bubbles oscillate independently. These oscillators have slightly different frequencies, resulting in two distinct lines in the spectrogram. We see both of these lines in the heater's temperature; each corresponds to the periodic cooling effect of their respective oscillating bubbles. This cooling effect is an important proof certifying that the bubbles are indeed oscillating in the stable mode.

Figure 10 presents the spectrogram of the acoustic emission and heater's temperature when two bubbles synchronize. The acoustic signal shows all four stages of the system: the initial explosion with a vertical burst, the independent oscillation with two separate frequency lines, the synchronization where only one frequency remains, and finally the growing and merging with dying oscillation. These patterns however are not reflected in the heater's temperature. After the first millisecond for the bubbles to adjust their sizes and choose their dynamics, no signal appears on the heater's spectrogram. Looking very carefully, we can see a thin line whose intensity is comparable to the noise level. This faint line might come from the cold (hot) circle of the inner gas as the bubble

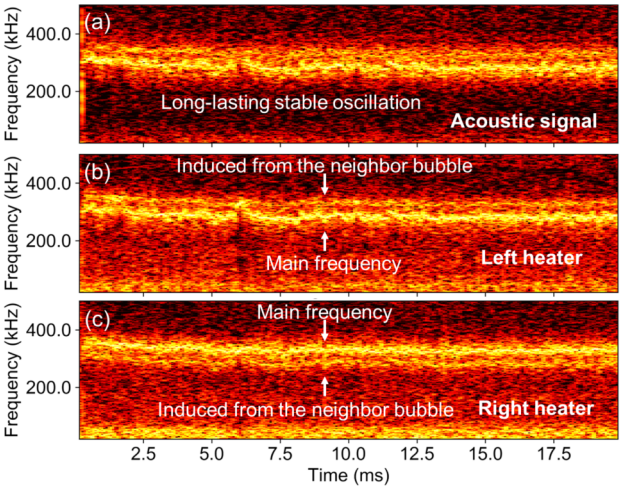

FIG. 9. Spectrograms of the (a) emitted acoustic signal, (b) temperature of the left heater, and (c) temperature of the right heater when two bubbles oscillate independently. These results are from the same experiment as in Fig. 4.

expands (collapses) and most likely is not relevant to the periodic liquid jet cooling in the case of the stable oscillation mode. Thus, it can be concluded that the bubbles in this case are oscillating in the unstable mode with neither microbubble pinch-off nor liquid-jet impact.

APPENDIX B: DETAILS ON NUMERICAL SIMULATIONS

1. Preprocessing step for the k-nearest-neighbor algorithm

The regions constructed in Fig. 6 are calculated using the k-nearest-neighbor algorithm [25] with $k = 5$. Prior to this calculation, a standard scaler is applied to each attribute of the data set. For each

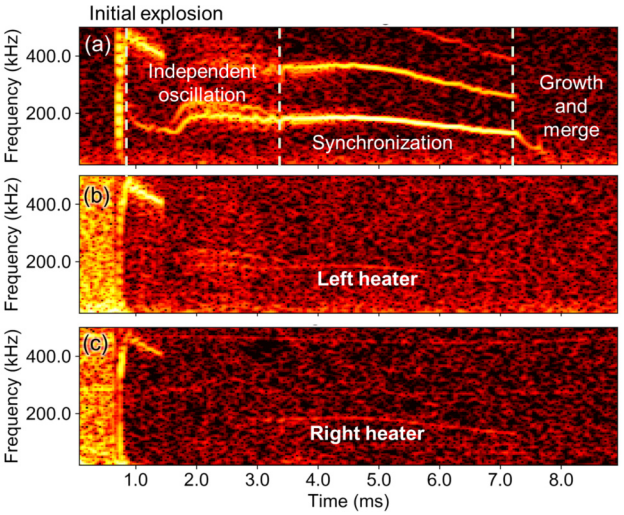

FIG. 10. Spectrograms of the (a) emitted acoustic signal, (b) temperature of the left heater, and (c) temperature of the right heater when two bubbles synchronize. These results are from the same experiment as in Fig. 3.

heating power datum P_i, a normalized power P_i' is derived

$$P_i' = \frac{P_i - P_{\text{mean}}}{\sigma_P}, \tag{B1}$$

where P_{mean} and σ_P are the mean and standard deviation of the heating power data set. The same procedure is applied for each heater's distance data point d_i. As a result, two sets of normalized, nondimensional data P_i' and d_i' are obtained. The distance between two data points A and B is then calculated as

$$D_{AB} = \sqrt{(P_A' - P_B')^2 + (d_A' - d_B')^2}, \tag{B2}$$

which is then used to find the nearest data points. The value $k = 5$ is chosen as it is the smallest value that leads to the formation of three distinct regions in the parameters space and also gives the highest accuracy.

2. Analytical model of the bubble dynamics

The model for the dynamics of oscillate-boiling bubble was reported in a previous study [23]. There the Keller-Miksis equation is coupled with the energy equation for the inner gas or vapor

$$dQ = pdV + dU \tag{B3}$$

to solve for the bubble's instantaneous radius and temperature. Here dQ is the total thermal energy received, p is the bubble's pressure, V is the bubble's radius, and U is the bubble's potential energy. In the case of stable oscillate boiling, to mimic the liquid jet impact, the heating power supplied to the bubble (which appears in the term dQ) is approximated to a step function. When the radius is smaller than a threshold value, indicating the point of collapse with the jet touching the heating substrate, the bubble receives full power from the heater and zero otherwise. With this power profile, the bubbles show a stable oscillation with fixed maximum radius and frequency after a few cycles (blue lines in Fig. 11).

In unstable oscillation where there is no jet impact, the smoother heat transfer is approximated to be inversely proportional to the bubble radius. The reason for this approximation is that without the jet impact, heat is transferred to the bubble via conduction through the inner gas or vapor. As the radius increases, the thermal conductance is reduced and the bubble receives less power. With this power profile, there is a decay in the oscillation amplitude. The bubble's radius is bigger and its frequency is lower compared to stable oscillate boiling (green lines in Fig. 11). These behaviors and the values of the bubbles' radii are in good agreement with the experimental results.

3. Simulation of the heater's thermal profile

Figure 12 shows the simulation domain used to calculate the thermal profile of the heating substrate presented in Fig. 8. To reduce computational cost, this domain only includes a small area ($500 \times 0.5\ \mu\text{m}^2$) surrounding the heaters. The thickness of the water column is 100 μm and of the glass substrate 30 μm. To solve for the thermal profile, first the current density $\mathbf{J}$ in the circuit is calculated

$$\mathbf{J} = \sigma \mathbf{E} = -\sigma \nabla V. \tag{B4}$$

Here σ is the electrical conductivity of the material and $\mathbf{E}$ is the vector electric field, which is obtained from the electrical potential V. The current density is then used to calculate the Joule heating per unit volume

$$P_{\text{Joule}} = \mathbf{J} \cdot \mathbf{J}/\sigma, \tag{B5}$$

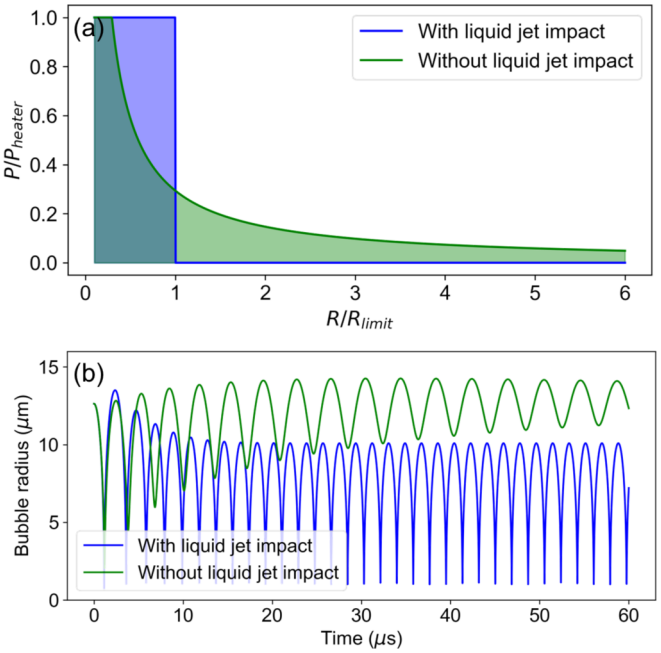

FIG. 11. (a) Power profile used in two cases: with liquid jet impact (stable oscillate boiling) and without liquid jet impact (unstable oscillate boiling). (b) Corresponding calculated bubble dynamics.

which is later used as the heat source in the thermal energy equation to solve for temperature

$$\rho C \frac{\partial T}{\partial t} - \nabla \cdot (k \nabla T) = P_{\text{Joule}}. \tag{B6}$$

Here ρ, C, and k are the material's density, heat capacity, and thermal conductivity, respectively. Equations (B1)–(B3) are solved at each time step using the finite-element method with commercial software COMSOL MULTIPHYSICS. The temperature at the boundary is set at room temperature. The electrical potential at one side of the gold electrode is set to fit the experimental values and at the other side to ground.

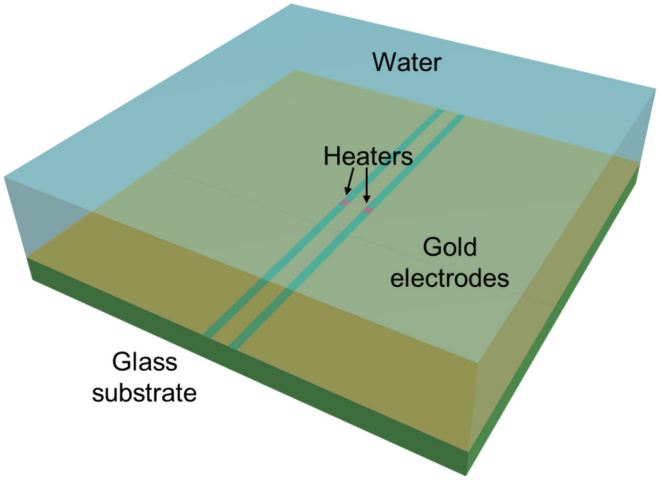

FIG. 12. Geometry of the simulation for the thermal profile of the heating substrates.

[1] W. Lauterborn and E. Cramer, Subharmonic Route to Chaos Observed in Acoustics, Phys. Rev. Lett. **47**, 1445 (1981).
[2] U. Parlitz, R. Mettin, S. Luther, I. Akhatov, M. Voss, and W. Lauterborn, Spatio-temporal dynamics of acoustic cavitation bubble clouds, Philos. Trans. R. Soc. A **357**, 313 (1999).
[3] D. Fernandez Rivas, A. Prosperetti, A. G. Zijlstra, D. Lohse, and H. J. G. E. Gardeniers, Efficient sonochemistry through microbubbles generated with micromachined surfaces, Angew. Chem. Int. Ed. **49**, 9699 (2010).
[4] D. F. Rivas, L. Stricker, A. G. Zijlstra, H. J. G. E. Gardeniers, D. Lohse, and A. Prosperetti, Ultrasound artificially nucleated bubbles and their sonochemical radical production, Ultras. Sonochem. **20**, 510 (2013).
[5] L. A. Crum, Bjerknes forces on bubbles in a stationary sound field, J. Acoust. Soc. Am. **57**, 1363 (1975).
[6] H. N. Oguz and A. Prosperetti, A generalization of the impulse and virial theorems with an application to bubble oscillations, J. Fluid Mech. **218**, 143 (1990).
[7] A. A. Doinikov and S. T. Zavtrak, On the mutual interaction of two gas bubbles in a sound field, Phys. Fluids **7**, 1923 (1995).
[8] R. Mettin, I. Akhatov, U. Parlitz, C. D. Ohl, and W. Lauterborn, Bjerknes forces between small cavitation bubbles in a strong acoustic field, Phys. Rev. E **56**, 2924 (1997).
[9] T. Barbat, N. Ashgriz, and C.-S. Liu, Dynamics of two interacting bubbles in an acoustic field, J. Fluid Mech. **389**, 137 (1999).
[10] A. A. Doinikov, Translational motion of two interacting bubbles in a strong acoustic field, Phys. Rev. E **64**, 026301 (2001).
[11] A. Harkin, T. J. Kaper, and A. Nadim, Coupled pulsation and translation of two gas bubbles in a liquid, J. Fluid Mech. **445**, 377 (2001).
[12] N. A. Pelekasis, A. Gaki, A. Doinikov, and J. A. Tsamopoulos, Secondary Bjerknes forces between two bubbles and the phenomenon of acoustic streamers, J. Fluid Mech. **500**, 313 (2004).
[13] V. Garbin, B. Dollet, M. Overvelde, D. Cojoc, E. Di Fabrizio, L. van Wijngaarden, A. Prosperetti, N. de Jong, D. Lohse, and M. Versluis, History force on coated microbubbles propelled by ultrasound, Phys. Fluids **21**, 092003 (2009).
[14] W. Lauterborn and T. Kurz, Physics of bubble oscillations, Rep. Prog. Phys. **73**, 106501 (2010).
[15] L. Stricker, B. Dollet, D. Fernández Rivas, and D. Lohse, Interacting bubble clouds and their sonochemical production, J. Acoust. Soc. Am. **134**, 1854 (2013).
[16] X. Xi, F. Cegla, R. Mettin, F. Holsteyns, and A. Lippert, Collective bubble dynamics near a surface in a weak acoustic standing wave field, J. Acoust. Soc. Am. **132**, 37 (2012).
[17] T. J. A. Kokhuis, V. Garbin, K. Kooiman, B. A. Naaijkens, L. J. M. Juffermans, O. Kamp, A. F. W. van der Steen, M. Versluis, and N. de Jong, Secondary Bjerknes forces deform targeted microbubbles, Ultrasound Med. Biol. **39**, 490 (2013).
[18] F. Hamaguchi and K. Ando, Linear oscillation of gas bubbles in a viscoelastic material under ultrasound irradiation, Phys. Fluids **27**, 113103 (2015).
[19] N. Sugita and T. Sugiura, Nonlinear normal modes and localization in two bubble oscillators, Ultrasonics **74**, 174 (2017).
[20] J. T. Tervo, R. Mettin, and W. Lauterborn, Bubble cluster dynamics in acoustic cavitation, Acta Acust. Acust. **92**, 178 (2006).
[21] A. Pikovsky, M. Rosenblum, and J. Kurths, *Synchronization: A Universal Concept in Nonlinear Sciences* (Cambridge University Press, Cambridge, 2003), Vol. 12, p. 14.
[22] D. M. Nguyen, L. Hu, J. Miao, and C.-D. Ohl, Oscillate Boiling from Electrical Microheaters, Phys. Rev. Appl. **10**, 044064 (2018).
[23] F. Li, S. R. Gonzalez-Avila, D. M. Nguyen, and C.-D. Ohl, Oscillate boiling from microheaters, Phys. Rev. Fluids **2**, 014007 (2017).
[24] See Supplemental Material at http://link.aps.org/supplemental/10.1103/PhysRevFluids.4.043601 for additional simulation result, parameter space of bubble radius versus their distances, and experimental observations of two bubbles in a mixed mode.

[25] P. A. Devijver and J. Kittler, *Pattern Recognition: A Statistical Approach* (Prentice-Hall, Englewood Cliffs, 1982), pp. 69–127.

[26] N. Bremond, M. Arora, C.-D. Ohl, and D. Lohse, Controlled Multibubble Surface Cavitation, Phys. Rev. Lett. **96**, 224501 (2006).

[27] J. B. Keller and M. Miksis, Bubble oscillations of large amplitude, J. Acoust. Soc. Am. **68**, 628 (1980).

[28] O. Supponen, D. Obreschkow, M. Tinguely, P. Kobel, N. Dorsaz, and M. Farhat, Scaling laws for jets of single cavitation bubbles, J. Fluid Mech. **802**, 263 (2016).